International Journal of Nanomedicine

Dovepress
open access to scientific and medical research

Open Access Full Text Article

ORIGINAL RESEARCH

Hybrid curcumin–phospholipid complex-near-infrared dye oral drug delivery system to inhibit lung metastasis of breast cancer

This article was published in the following Dove Press journal:
International Journal of Nanomedicine

Ying Liu*
Peiwen Huang*
Xuefeng Hou
Fei Yan
Zifei Jiang
Jiangpei Shi
Xingmei Xie
Junyi Shen
Qiangyuan Fan
Zhi Wang
Nianping Feng

School of Pharmacy, Shanghai University of Traditional Chinese Medicine, Shanghai 201203, People's Republic of China

*These authors contributed equally to this work

Background: Oral route of administration is preferred for treating breast cancer, especially when continued disease management with good tolerability is required; however, orally administered chemotherapeutics combined with near-infrared (NIR) dyes are hindered by the low bioavailability, insufficient for the desired therapeutic efficacy. In this study, we developed a hybrid self-microemulsifying drug delivery system for co-loading curcumin–phospholipid complex and NIR dye IR780 (CUR/IR780@SMEDDS), to achieve combined phototherapeutic and chemotherapeutic effects against lung metastasis of breast cancer.

Methods: CUR/IR780@SMEDDS were characterized. The efficacy against breast cancer metastasis was evaluated by photothermal and photodynamic assessment, cytotoxicity, invasion, and migration in metastatic 4T1 breast cancer cells in vitro, and in vivo oral bioavailability study in rats and pharmacodynamics studies in tumor-bearing nude mice.

Results: CUR/IR780@SMEDDS improved oral bioavailability of curcumin and IR780 in rats compared with curcumin and IR780 suspensions. CUR/IR780@SMEDDS exhibited remarkable photothermal and photodynamic effects in vitro. In metastatic 4T1 breast cancer cells, CUR/IR780@SMEDDS combined with localized NIR laser irradiation induced significant cytotoxicity and inhibited invasion and migration of 4T1 cells, an outcome attributable to cumulative effects of IR780-induced hyperthermia and pharmacological effects of curcumin. In orthotopic 4T1 tumor-bearing nude mice, combination of oral administration of CUR/IR780@SMEDDS with local NIR laser irradiation inhibited tumor progression and suppressed lung metastasis.

Keywords: curcumin, IR780, oral drug delivery, lung metastasis of breast cancer, photo/chemotherapy

Introduction

Metastatic breast cancer is a global, life-threatening neoplastic disease, with lung and bone metastases occurring in approximately 60% of breast cancer patients.[1] Poor prognosis of metastatic breast cancer is illustrated by an overall 5-year survival rate of approximately 27%.[2] Therefore, inhibiting tumor growth and metastasis and achieving long-term disease management remains a challenge in breast cancer therapy. Multiple treatment modalities for metastatic breast cancer have been developed, including chemotherapy,[3] radiotherapy,[4] phototherapy (photothermal and photodynamic therapy),[5,6] gene therapy,[7] and combination therapy.[8,9] Photothermal therapy is attractive because of its non-invasive nature, light-triggered anticancer effects, and spatial/temporal selectivity. Additionally,

Correspondence: Nianping Feng
Department of Pharmaceutical Sciences, School of Pharmacy, Shanghai University of Traditional Chinese Medicine, 1200 Cailun Road, Zhangjiang Hi-Tech Park, Pudong New District, Shanghai 201203, People's Republic of China
Tel +86 215 132 2198
Fax +86 215 132 2198
Email npfeng@hotmail.com

submit your manuscript | www.dovepress.com
DovePress
http://doi.org/10.2147/IJN.S200847

compared to radiotherapy, phototherapy inflicts less damage to surrounding tissues and the patient body. Photothermal agents convert light to thermal energy by absorbing near-infrared (NIR) radiation, using hyperthermia to kill tumor cells.[10] In contrast, photosensitizers, upon exposure to specific light wavelengths, generate ROS, leading to tumor cell apoptosis.[11] IR780 is a stable, highly fluorescent NIR dye used in phototherapy and capable of producing hyperthermia and ROS. IR780 is transported by organic anion transporter polypeptides and can therefore accumulate in many tumor types including breast cancer and achieve tumor targeting, a feature beneficial for oral IR780 delivery.[12–15] Phototherapy was effective in inhibiting proliferation and inducing tumor cell death at the primary lesion. However, after tumor recurrence, in general, survival rate of patients decreases greatly. Combination of chemo- and photothermal therapy was more effective than either therapy alone.[16–18] Given IR780's potent photothermal efficacy and suitability for oral administration, the dye is expected to exhibit improved therapeutic efficacy against metastatic breast cancer when combined with oral chemotherapeutics. More importantly, the combination is expected to reduce the administration dose of IR780, which is great beneficial to reduce the potential toxicity of IR780 at high dose in vivo.

Curcumin is the main active ingredient of *Curcuma longa* and potentially suppresses breast cancer progression. Curcumin has shown promising effects in inhibiting cancer angiogenesis, cell migration, and invasion by interacting with NF-κB,[19] a key regulatory molecule of cancer progression and metastasis. Additionally, curcumin modulates the expression of multiple cell signaling proteins, such as NF-κB, COX-2, and MMP9[20] and inhibits epithelial–mesenchymal transition.[21] Despite great promise of curcumin in metastatic breast cancer treatment, hydrophobicity in alkaline conditions, photodegradable, poor absorption, rapid metabolism and elimination, short half-life, and low and variable bioavailability have hindered its clinical application.[22–25]

Recently, oral delivery of anticancer agents has gained increasing attention. Compared to intravenous administration, oral delivery of anticancer agents is non-invasive and cost-effective; it simplifies therapeutic procedures, improves patient life quality and compliance, and offers good tolerability.[26] Additionally, it is well suited for maintenance treatment and prolonged disease control.[27] However, oral delivery systems are in challenged by physiological and biochemical barriers and by physiochemical properties of anticancer drugs.[28] To overcome these issues, numerous nanocarriers have been rationally designed in the last decade,[29–32] improving bioavailability and enhancing therapeutic efficacy.

Self-microemulsifying drug delivery systems (SMEDDSs) have been intensively investigated to improve oral bioavailability of poorly water-soluble drugs.[31,32] However, few oral nanocarriers carrying chemotherapeutics and NIR dyes and combining the benefits of chemo- and phototherapy have been investigated for metastatic breast cancer treatment. IR780 and curcumin may interact via π–π stacking, facilitating the accommodation of IR780 in SMEDDS, which improves their oral absorption and bioavailability. Curcumin acts as a chemotherapeutic, inhibiting the progression of metastatic breast cancer, whereas IR780, after NIR irradiation, exerts photothermal effects and promotes ROS generation. In this study, we evaluated the potential of CUR/IR780@SMEDDS as an oral drug delivery system for metastatic breast cancer treatment using in vitro cell models and xenograft tumor nude mice models.

Methods

Materials

Curcumin (purity>98%) was purchased from Dalian Meilun Biotechnology Co. Ltd (Dalian, People's Republic of China). IR780 (2-[2-[2-chloro-3-[(1,3-dihydro-3,3-dimethyl-1-propyl-2*H*-indol-2-ylidene)ethylidene]-1-cyclohexen-1-yl] ethenyl]-3,3-dimethyl-1-propylindolium iodide) was purchased from Sigma Aldrich (St. Louis, MO, USA). Soya bean lecithin (S100) were obtained from A.V.T. Pharmaceutical Co. Ltd (Shanghai, People's Republic of China). Oleoyl macrogol-6/polyoxyl-6 glycerides (Labrafil® M1944 CS), PEG-40 hydrogenated castor oil (Cremophor RH40®), and caprylocaproyl macrogol-8 glycerides (Labrasol®) were kindly gifted by Gattefossè, Gennevilliers, France. Chemicals and solvents were of analytical or chromatographic grade. 4T1 and Caco-2 cell lines were supplied by the Institute of Biochemistry and Cell Biology (Shanghai, People's Republic of China).

Preparation and characterization of CUR/IR780@SMEDDS

Curcumin, IR780, and phospholipids were dissolved in ethanol. After stirring at 37°C for 3 hrs, the solvent was evaporated using a rotary evaporator. The obtained complex was mixed with Labrasol, before adding Labrafil M1944 CS and Cremophor RH40 at 37°C and stirring the mixture until

a transparent liquid formed. To study the droplet size, size distribution and ζ-potential of CUR/IR780@SMEDDS, 100 μL of prepared CUR/IR780@SMEDDS were slowly dropped into the 10 mL 37°C water, stirring with a speed of 100 rpm to form microemulsions. CUR/IR780@SMEDDS microemulsions samples were tested using a Zetasizer detector to determine droplet size, size distribution, and ζ-potential.[33,34]

Cumulative in vitro release of curcumin and IR780

Release profiles of curcumin and IR780 from CUR/IR780@SMEDDS were investigated using the dialysis bag method. CUR/IR780@SMEDDS containing 1.0 mg of curcumin was loaded into the dialysis bag, which was incubated in 1.0 mL PBS (pH 6.8) and shaken at 100 rpm and 37°C. At predetermined time intervals, 500 μL of the release medium were collected and replaced with the same volume of fresh PBS (pH 6.8). The released curcumin was measured by HPLC, whereas IR780 content was determined using UV-Vis spectrophotometry. All experiments were performed in triplicate.

Photothermal properties of CUR/IR780@SMEDDS in vitro

CUR/IR780@SMEDDS was diluted with ultrapure water to the final IR780 concentrations of 30 and 50 μg/mL. Samples (1 mL) were added to a 24-well plate, with 1 mL of deionized water and curcumin–phospholipid complex-loaded self-microemulsifying drug delivery system (CUR@SMEDDS) used as controls. The wells were irradiated (808 nm, 0.8 W/cm^2) for 5 mins and the temperature was recorded at 30 s intervals using a thermal probe. All experiments were performed in triplicate.

To investigate thermogenic capacity, thermal photos were taken during laser irradiation. CUR/IR780@SMEDDS was diluted with ultrapure water to the final IR780 concentration of 50 μg/mL. Samples and CUR@SMEDDS as negative controls were irradiated (808 nm, 0.8 W/cm^2) for 5 mins and thermal infrared images were captured every 30 s using an infrared-seek thermal imaging camera.

Cellular uptake

Cellular uptake of SMEDDS was investigated using confocal laser scanning microscopy. As curcumin fluoresces, no additional fluorescent indicators were used. Caco-2 or 4T1 cells were cultured in glass-bottom cell culture dishes at a density of 1×10^4 cells per well. After overnight culture, the cells were treated with 1 mL of CUR/IR780@SMEDDS (containing 6 μg/mL curcumin and 3 μg/mL IR780) for 1, 2, and 4 hrs at 37°C. Afterward, the cells were repeatedly washed with PBS, fixed with 4% paraformaldehyde for 30 mins, and stained with DAPI. After washing three times with PBS, the cells were visualized using a TCS SP8 confocal system, at the following wavelengths: 405 nm (DAPI), 488 nm (curcumin excitation), 560–620 nm (curcumin emission), 638 nm (IR780 excitation), and 700–800 nm (IR780 emission).

In vitro anti-metastatic effects in 4T1 cells

Cell proliferation analysis

4T1 cells were seeded in a 96-well plate at the density of 1×10^4 cells per well. After 24-hr incubation, the cells were treated with control (untreated), control+NIR, blank SMEDDS, CUR@SMEDDS, IR780, CUR@SMEDDS+NIR, CUR/IR780@SMEDDS, and CUR/IR780@SMEDDS+NIR for 12 hrs, with each treatment repeated in six wells. After washing the cells three times with PBS, the media were replaced with MTT solution (5 mg/mL) for 4 hrs. After dissolv ing formazan crystals in DMSO, cell viability was determined using a microplate reader at 570 nm.

Wound healing assay

Wound healing assay was performed to investigate the effect of CUR/IR780@SMEDDS on migratory potential of 4T1 cells, as previously described.[35] Briefly, 8×10^5 cells were seeded in 6-well culture plates and cultured overnight. Wounds were generated with a 200 μL pipette tip and the cells were treated with control, control+NIR, IR780, CUR@SMEDDS, IR780+NIR, CUR/IR780@SMEDDS, and CUR/IR780@SMEDDS+NIR with curcumin and IR780 concentrations of 10 and 5 μg/mL, respectively. Cell images were captured. The wound area was calculated using ImageJ software.

In vitro migration and invasion assay

4T1 cells were seeded in a 6-well culture plate and cultured for 24 hrs. The cells were treated with control, control+NIR, IR780, CUR@SMEDDS, IR780+NIR, CUR/IR780@SMEDDS, and CUR/IR780@SMEDDS+NIR (curcumin, 6 μg/mL; IR780, 3 μg/mL). After 12 hrs, the cells were washed twice with PBS and the NIR group was exposed to laser irradiation (808 nm, 0.8 W/cm^2). The cells were suspended in serum-free culture medium and in vitro transwell migration and invasion assays were performed, as previously

described.[36] Briefly, 1×10^5 cells were seeded to the top chambers of 24-well transwell inserts without a gel-coated membrane for the transwell migration assay, whereas for the invasion assay, 1×10^5 cells were seeded in the top chamber with a Matrigel-coated membrane, supplemented with no serum medium. In both assays, the lower chambers were filled with 600 μL medium supplemented with serum. After a 24-hr incubation, cells remaining in the top chamber were removed with a cotton swab. The cells that migrated through the filters into the lower wells were fixed with 90% ethanol for 20 mins, stained with crystal violet for 20 mins, and photographed. For quantification, the crystals were dissolved in 35% acetic acid solution and the samples were analyzed using a microplate reader.

ROS detection in vitro

Photodynamic efficacy of CUR/IR780@SMEDDS was evaluated by determining ROS production in 4T1 cells, as previously described.[37] 1×10^4 4T1 cells were seeded into a glass-bottom culture dish. After 24-hr incubation, the cells were treated with CUR/IR780@SMEDDS (curcumin, 10 μg/mL; IR780, 5 μg/mL) containing H_2DCFDA (40 mM). Blank culture medium was used as control. The cells were incubated for 4 hrs at 37°C, rinsed with PBS, and irradiated using a NIR laser (808 nm, 0.8 W/cm^2) for 5 mins per well. Control cell groups received no irradiation and were not treated with SMEDDS. Fluorescence images were immediately observed using confocal laser scanning microscopy.

In vivo bioavailability

The animals were housed under standard laboratory conditions and given access to sterile food and clean water ad libitum. All animal experiments were conducted and approved by Animal Care and Use Committee of Shanghai University of Traditional Chinese Medicine. The experimental procedures were in compliance with the National Institutes of Health Guide for Care and Use of Laboratory Animals. Tumor-free Sprague Dawley rats (200 ±20 g) were randomly divided into CUR/IR780@SMEDDS, curcumin suspensions, IR780 suspensions (n=5). Curcumin and IR780 suspensions were prepared by dispersing curcumin and IR780 in 0.5% carboxymethyl cellulose solution. The animals were orally administered a single dose of 75 mg/kg curcumin and 10 mg/kg IR780. Blood samples were collected from the orbital vein at 15, 30, 60, 90, 120, 240, 360, 480, 720, 1,440, 2,880 mins after oral administration and centrifuged at 1,800 *g* for 5 mins. Curcumin and IR780 content in the serum samples were separately determined using LC-MS and Varioskan Flash Spectral Scanning multimode plate reader. LC-MS was performed on an Ultimate 3000 UPLC system (Thermo, USA) using an Hypersil GOLD C18 column (2.1 mm×50 mm, 3 μm, Thermo, USA). The analysis was achieved with gradient elution using (A) acetonitrile and (B) water (containing 0.5% formic acid) as the mobile phase (A:B=68:32, v/v). A TSQ triple-quadrupole tandem mass spectrometer (Thermo, USA) in positive HESI mode was used. The conditions are as follows: capillary voltage, 2,800 V; vaporizer temperature, 80°C; capillary temperature, 350°C. Selective reaction monitor (SRM) of the transitions of m/z 367.1→272.9 for curcumin. For collision-induced dissociation, argon was used as the collision gas at a flow rate of 0.20 mL/min.

In vivo imaging and biodistribution studies

In order to evaluate tumor retention of CUR/IR780@SMEDDS and biodistribution, 4T1 breast cancer models were constructed in BALB/c nude mice (20±2 g). Tumor xenografts were imaged at the tumor size of approximately 500 mm^3. The mice were orally administered CUR/IR780@SMEDDS and IR780 suspension at IR780 dose of 6.5 mg/kg; mice receiving normal saline were used as control. After 1, 2, 4, 6, 8, 24, and 48 hrs, in vivo imaging using IVIS imaging system was performed. After 48 hrs, the mice were sacrificed and biodistribution of IR780 in mice organs was evaluated.

In vivo therapeutic efficacy against metastatic breast cancer

4T1 cells (1×10^6) were directly injected into the second pair of mammary pads of 4-week-old BALB/c nude mice to establish breast cancer models. 4T1 tumor-bearing mice were randomly divided into seven groups after tumors reached approximately 150 mm^3 (n=7) and were orally administered different formulations (control, IR780, CUR, IR780 +NIR, CUR/IR780@SMEDDS, CUR@SMEDDS, and CUR/IR780@SMEDDS+NIR) every 2 days for 16 days with dose of 50 mg/kg curcumin and 5 mg/kg IR780. Tumor volume and mice body weight were recorded. Mice tumors were irradiated (0.8 W/cm^2 at 808 nm for 5 mins with the area of irradiation spot of 66 mm^3) 24 hrs after each treatment. During irradiation, the temperature of tumors in control+NIR, IR780+NIR, and CUR/IR780@SMEDDS +NIR groups was recorded every 30 s and the tumors were

photographed using a thermal camera. On day 16, the mice were sacrificed and the pulmonary metastatic nodules were photographed and counted for the in vivo anti-metastatic assay. Tumors and organs were fixed with 10% paraformaldehyde and embedded into paraffin. The tissue blocks (superficial and deep tissue regions) were cut and stained with H&E and analyzed using terminal deoxynucleotidyl transferase dUTP nick end labeling (TUNEL assay).

Preliminary safety evaluation in mice

BALB/c mice were randomly divided into two groups (n=5) and orally received saline (as control) or CUR/IR780@SMEDDS with dose of 50 mg/kg curcumin and 5 mg/kg IR780 every 2 days for 16 days. On day 16, the mice were sacrificed to collect blood samples, stomach, and intestines for further blood biochemistry analyses, hematological analysis, and histological H&E staining.

Statistical analysis

Data are expressed as means±SD of at least three independent experiments. Statistical analysis was performed using Student's *t*-test and one-way ANOVA for pairs of samples. *p*-values <0.05 were considered statistically significant.

Results and discussion

Preparation and characterization of CUR/IR780@SMEDDS

In this study, an oral SMEDDS-based nanocarrier was developed for co-loading of curcumin and IR780 (Figure 1A), with the purpose of achieving combined photo- and chemotherapy of metastatic breast cancer. Curcumin–phospholipid complexes were prepared by solvent evaporation as previously described,[38] based on interaction of phospholipids with curcumin in an aprotic solvent. Drug-phospholipid complexes are formed via electrostatic interactions, hydrogen bonds, and van der Walls forces.[39] Complex formation was confirmed by Fourier transform infrared spectroscopy (FTIR) spectroscopy (Figure1B). Curcumin exhibited characteristic hydroxyl stretching band at 3,504 cm^{-1}, which weakened considerably in the complex spectrum. Additionally, phospholipid showed peaks at 1,249 cm^{-1} (*P*=O stretching), which shifted to 1,254 and 1,284 cm^{-1} in curcumin–phospholipid physical mixture and complex spectra, respectively, possibly because of the complexation between the hydroxy and the *P*=O group. Curcumin–phospholipid complex has been previously reported.[40,41] Whether IR780 can form a complex with phospholipids or only interacts with curcumin was initially unclear; however, in this study, IR780 did not form a complex with the phospholipid (Figure S1). Curcumin structure incorporates an extensive aromatic π-electron system (Figure 1C), which allows strong π-π stacking interactions with aromatic molecules, whereas IR780 features a rigid cyclohexenyl ring in the heptamethine chain.[42] Thus, we propose that curcumin co-assembles with IR780 via π–π stacking interactions. To verify this hypothesis, we analyzed fluorescence quenching by comparing the changes in the emission spectra of curcumin and IR780 with changes in compound concentration. As shown in Figure 1E and F, fluorescence intensity of curcumin and IR780 gradually decreased with increasing IR780 and curcumin concentrations, indicating fluorescence quenching and suggesting the existence of interactions between curcumin and IR780.

The SMEDDS formulation was designed by determining solubility and constructing a pseudoternary phase diagram. Labrafil M1944 CS, Cremophor RH40, and Labrasol (2:1:1, w/w/w) were selected as the oil phase, surfactant, and co-surfactant, respectively, as these excipients dissolved both curcumin and IR780 and showed promising self-microemulsifying efficiency. Additionally, in the absence of curcumin–phospholipid complex, IR780 loaded into the blank SMEDDS failed to form a stable microemulsion, indicating the significance of interaction between curcumin and IR780 in CUR/IR780 formation. Furthermore, the interaction between curcumin and IR780 in SMEDDS was also revealed by the absorption spectra of CUR/IR780@SMEDDSs (Figure 1G). Due to the interference of phospholipids on the curcumin absorption determination (as shown in the inset figure at the upper right corner), it is difficult to judge the absorption peak shift of curcumin in the spectrum of CUR/IR780@SMEDDSs compared with the raw curcumin. However, compared with raw IR780, CUR/IR780@SMEDDSs exhibited clear red shift of the absorption peak of IR780 from 784 to 792 nm, suggesting the presence of interaction between curcumin and IR780 in SMEDDS.

The prepared CUR/IR780@SMEDDSs particles were spherical and displayed a narrow size distribution, as shown in the transmission electron microscopy image (Figure 1D). Hydrodynamic size of CUR/IR780@SMEDDS dispersed in deionized water determined by dynamic light scattering was 38.26±0.25 nm (Figure 1D), suitable for oral administration and absorption through the gastrointestinal tract. Self-emulsifying time of the formulation was <3 mins. Drug loading increased droplet size compared to particle sizes of drug-free preparations and the final formulation was further optimized for use in this study.

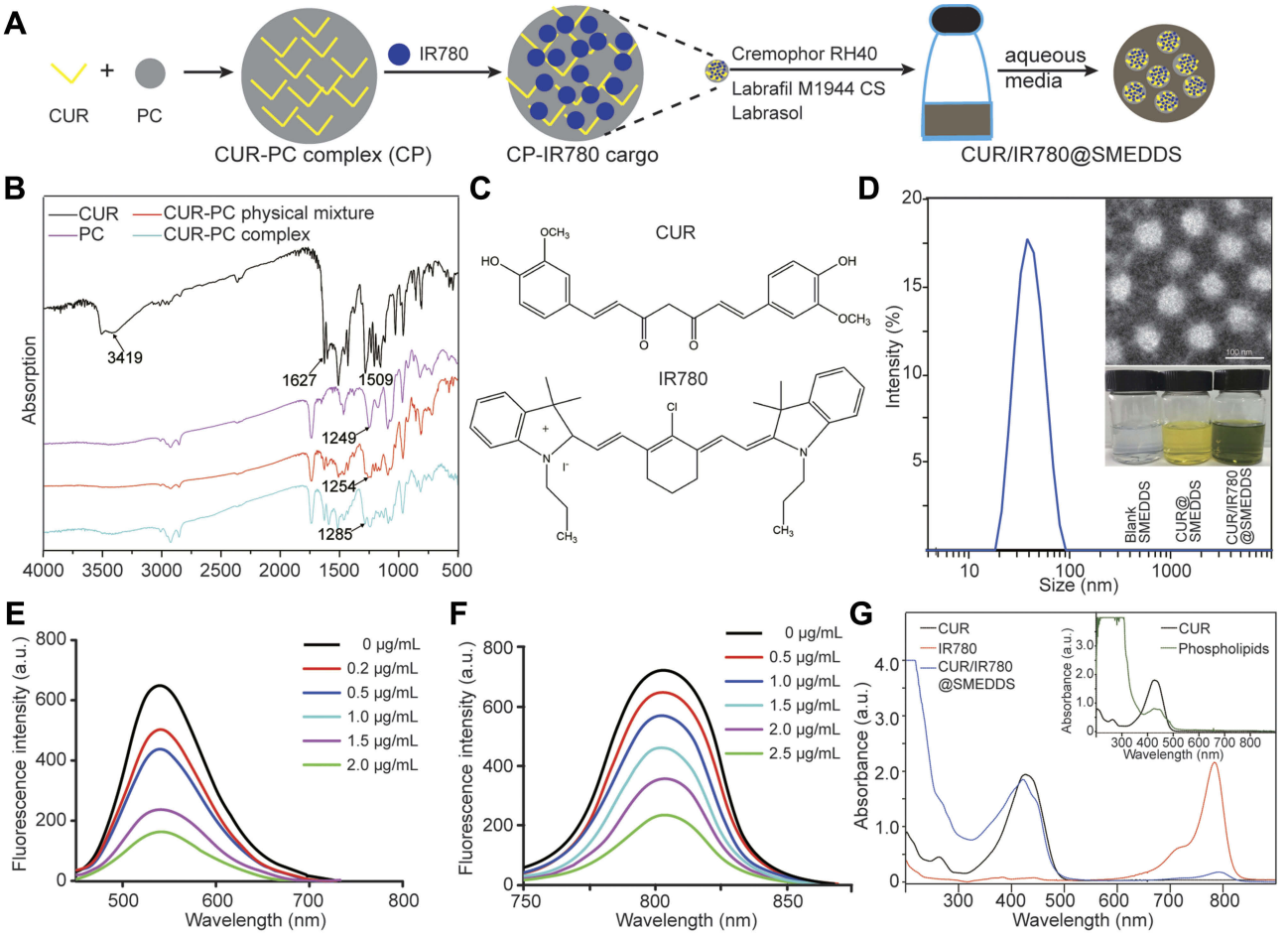

Figure 1 (**A**) Schematic illustration of preparation of the curcumin–phospholipid complex and IR780-loaded self-microemulsifying drug delivery systems. (**B**) FTIR spectra of curcumin (CUR), phospholipid (PC), physical mixture of CUR and PC (CUR-PC physical mixture), and CUR-PC complex. (**C**) Chemical structures of CUR and IR780. (**D**) Droplet size of CUR/IR780@SMEDDS. Insert: TEM image of CUR/IR780@SMEDDS (upper panel) and photograph of blank SMEDDS, CUR@SMEDDS, and CUR/IR780@SMEDDS (lower panel). (**E**) Fluorescence emission spectra of CUR in the presence of different IR780 concentrations. (**F**) Fluorescence emission spectra of IR780 in the presence of different CUR concentrations. (**G**) UV-Vis absorption spectra of CUR, phospholipids, IR780, and CUR/IR780@SMEDDS.

Release of curcumin and IR780 from SMEDDS was analyzed in vitro without laser irradiation. Because of limited solubility of curcumin in PBS, 50% ethanol was used as the release medium to provide the sink condition. In the first 3 hrs, 41.6% curcumin and 55.1% IR780 was released from CUR/IR780@SMEDDS, whereas approximately 89.9% of curcumin (Figure 2A) and 92.1% of IR780 (Figure 2B) was released from SMEDDS in 24 hrs. To get clearly understand the release and stability in stomach, in future, it would be beneficial to study the release of SMEDDS in acidic pH, and reveal its behavior in the stomach.

Photothermal and photodynamic effects of CUR/IR780@SMEDDS

In order to evaluate photothermal properties of CUR/IR780@SMEDDS, we monitored temperature changes upon laser irradiation (808 nm, 0.8 W/cm^2). As shown in Figure 2C, negative control (deionized water) and CUR@SMEDDS showed a temperature increase of approximately 4°C. In contrast, in aqueous dispersions of CUR/IR780@SMEDDS at different concentrations, temperature increased gradually and reached a plateau for the concentration of 30 μg/mL, increasing by approximately 15°C after 5-min irradiation (Figure 2C). In addition, the rate of temperature increase in aqueous dispersions of CUR/IR780@SMEDDS rapidly increased with higher concentrations of the preparation, corresponding to higher IR780 content.

Furthermore, photos and thermal images of CUR/IR780@SMEDDS were taken to observe the changes in temperature during exposure to 808 nm laser irradiation. As shown in Figure 2D, pseudo-color signals in the SMEDDS group grew stronger with irradiation time, indicating the increase in temperature, whereas almost no change in pseudo-color signals was observed in the control

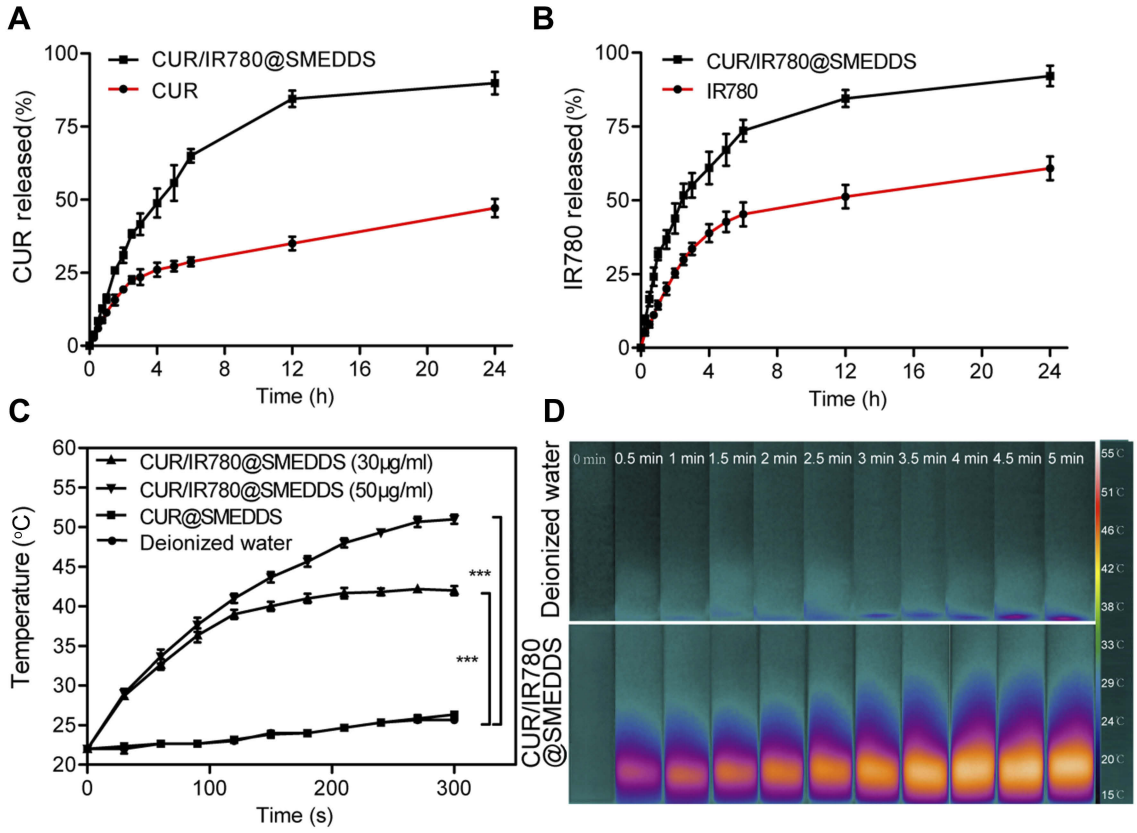

Figure 2 In vitro release profiles of curcumin (CUR) (**A**) and IR780 (**B**) in PBS (pH 6.8). (**C**–**D**) In vitro photothermal behavior of CUR/IR780@SMEDDS: (**C**) temperature change curves of CUR/IR780@SMEDDS containing different concentrations of IR780 after NIR irradiation (808 nm, 0.8 W/cm^2). CUR@SMEDDS and deionized water were used as control. (**D**) IR thermal images of deionized water and CUR/IR780@SMEDDS during 5-min laser irradiation. Data are represented as means±SD (n=3).

group. Taken together, these results suggest promising NIR photothermal capacity of CUR/IR780@SMEDDS.

In order to investigate ROS generation potential of CUR/IR780@SMEDDS upon exposure to NIR laser irradiation, we detected intracellular ROS generation using a redox-sensitive probe H_2DCFDA in 4T1 cells. No fluorescence signal was found in cells in control PBS and CUR/IR780@SMEDDS groups. However, green fluorescence was observed in cells treated with CUR/IR780@SMEDDS under NIR irradiation (Figure 4A, Figure S2), indicating ROS production. After NIR exposure, IR780 produces reactive molecules and the generated ROS possibly mediate photo-induced cytotoxicity.[43] Therefore, we attempted to correlate ROS generation and cell viability. CUR/IR780@SMEDDS treatment with exposure to NIR irradiation exhibited the highest cytotoxicity, consistent with high ROS production. This observation implies that ROS generated by CUR/IR780@SMEDDS upon laser irradiation may induce cellular death, in agreement with a previous report.[44] Additionally, in the ROS detection assay, CUR/IR780@SMEDDS treatment without NIR irradiation showed very light fluorescence compared to the control group (Figure 4B), which might be caused by intrinsic ROS generation capacity of curcumin.

In vitro cellular uptake and cytotoxicity analysis

Cellular uptake was evaluated in Caco-2 and 4T1 cells. As shown in confocal images in Figure 3, Figure S3, and Figure S4, fluorescence signal was shown in both cell lines. Red IR780 signal was distributed in cytoplasm, in line with a previous report.[37] Additionally, we evaluated the effects of NIR laser irradiation on cellular uptake in 4T1 cells. After incubation with NIR laser irradiation for 5 mins, cellular uptake increased, which may be attributed to improve movement and diffusion of nanoparticles in culture media at higher temperatures. Cellular uptake was also determined by flow cytometry. As shown in Figure 4C, NIR irradiation improved cellular uptake, in agreement with a previous report of photothermal effect promoting nanocarrier endocytosis and intracellular accumulation.[45]

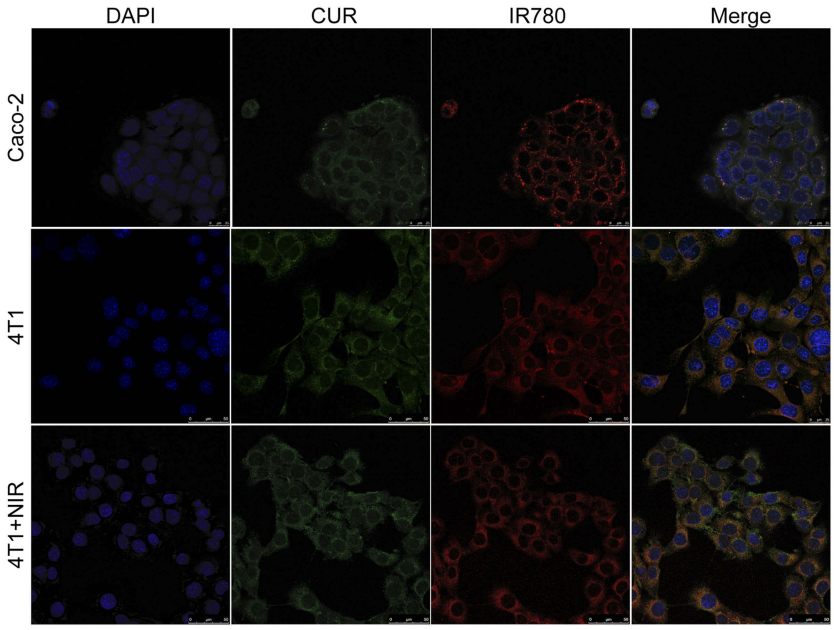

Figure 3 Confocal images of cellular uptake for CUR/IR780@SMEDDS in Caco-2 cells and 4T1 cells.

In vitro cytotoxicity of CUR/IR780@SMEDDSs in 4T1 cells was evaluated using the MTT assay (Figure 4D). Compared to IR780 treatment in the absence of NIR irradiation, IR780 under NIR irradiation significantly decreased 4T1 cell viability, indicating that NIR irradiation increased IR780 cytotoxicity. This result was consistent with previous findings[46] and possibly associated with cytotoxicity caused by temperature increase and increased ROS production upon irradiation. Similarly, decreased cell viability was observed after CUR/IR780@SEMDDS treatment combined with NIR irradiation, compared to cell viability after treatment with preparations in the absence of NIR irradiation. Furthermore, compared to CUR@SMEDDS, CUR/IR780@SMEDDS demonstrated significantly increased cytotoxicity, indicating additive cytotoxic effects of curcumin and IR780. Improved cytotoxicity of IR780 combined with chemotherapeutics such as doxorubicin was previously attributed to enhance cytotoxicity of doxorubicin with temperature increase and higher heat sensitivity of tumor cells exposed to doxorubicin.[46]

CUR/IR780@SMEDDS inhibits migration and invasion of 4T1 cells in vitro

To evaluate inhibition of breast cancer metastasis, we first investigated the effect of various formulations on 4T1 cell migration by wound healing assay (Figure 4E(a), Figure S5). Untreated cells and cells treated only with NIR irradiation migrated and filled the wound gap after 24 hrs (Figure 4E, panel (a)). In IR780 group, approximately 62% cell migration occurred, indicating that IR780 partially inhibits tumor cell migration, consistent with a previous report.[7] Additionally, wound healing was significantly inhibited by CUR@SMEDDS. Combining IR780 and curcumin in SMEDDS (CUR/IR780@SMEDDS) did not further inhibit migration, as shown in Figure 4E(a). We next examined the effects of NIR on cell migration. CUR/IR780@SMEDDS significantly inhibited cell migration after NIR irradiation, compared to treatments in the absence of NIR, revealing the potential of photothermal treatments in cell migration inhibition.

Inhibitory effects of CUR/IR780@SMEDDS on cell longitudinal migration were further confirmed by the transwell migration assay (Figure 4E(b) and F). As shown in Figure 4E (b), 72.5% and 49.6% of cells migrated from the upper to the lower chamber after free IR780 and CUR/IR780@SMEDDS treatments, respectively. As expected, after NIR exposure, fraction of migrating 4T1 cells reduced to 35.8% and 12.1%, indicating that NIR enhanced migration inhibition.

As invasion is a hallmark of breast cancer metastasis, we evaluated the effects of CUR/IR780@SMEDDSs on the invasive behavior of 4T1 cells (Figure 4E(c) and G). Cell invasion through Matrigel was inhibited 48.5% by CUR/IR780@SMEDDS, suggesting that, in agreement with the results of the migration assays, CUR/IR780@SMEDDS reduced the invasive capacity of 4T1 cells. NIR irradiation greatly enhanced the effect (cell invasion rate of 6.1%). It has been reported that curcumin may suppress migration and

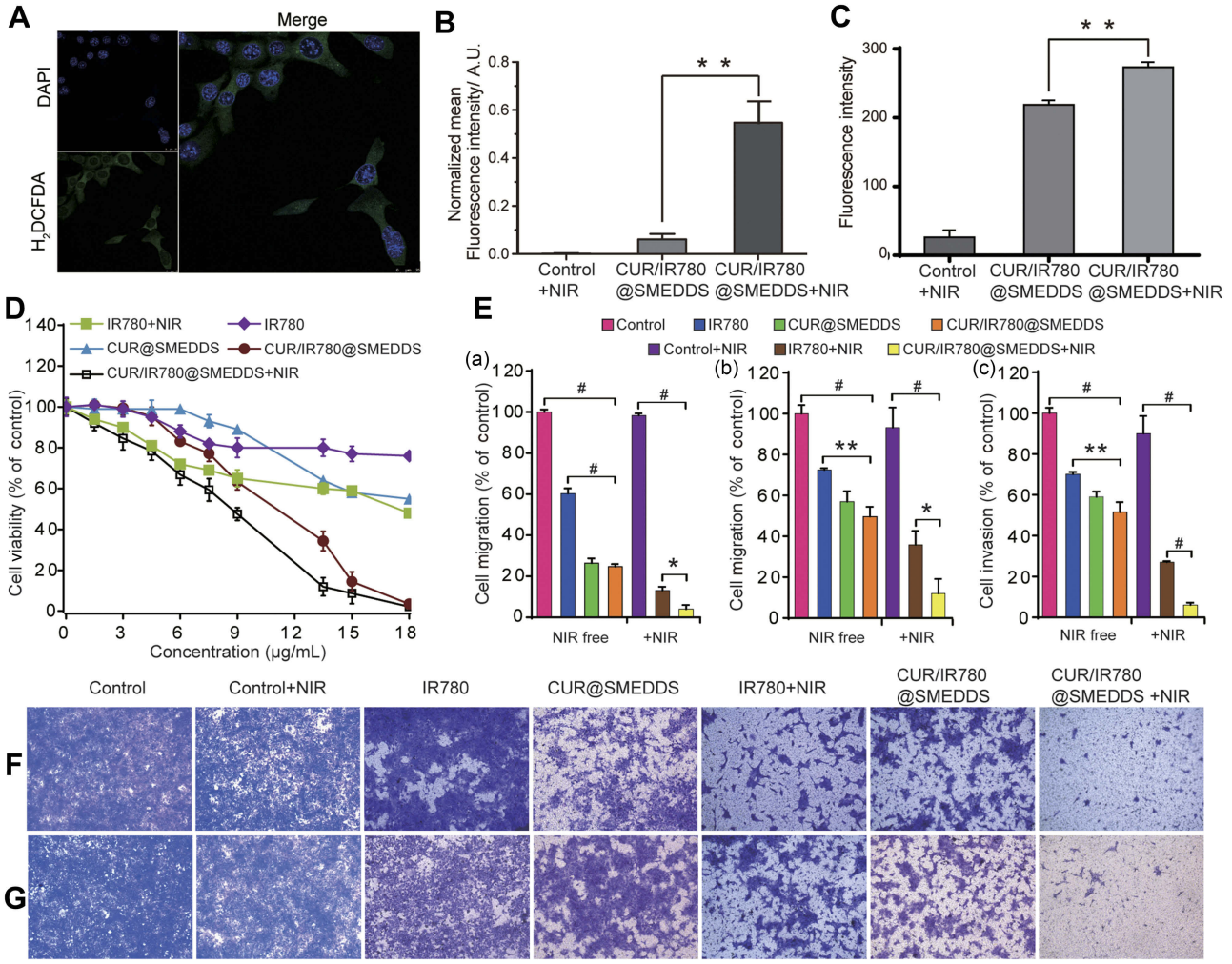

Figure 4 (**A**) Confocal images of ROS generation by CUR/IR780@SMEDDS after NIR irradiation (808 nm, 0.8 W/cm^2, 5 mins) in 4T1 cells. (**B**) Quantitative analysis of ROS generation by PBS (control), CUR/IR780@SMEDDS, and CUR/IR780@SMEDDS after NIR irradiation (808 nm, 0.8 W/cm^2, 5 mins) in 4T1 cells. (**C**) In vitro cellular uptake of control, CUR/IR780@SMEDDS, and CUR/IR780@SMEDDS+NIR. ** p<0.01. (**D**) Cell viability of 4T1 cells incubated with IR780, CUR@SMEDDS, CUR/IR780@SMEDDS, IR780+NIR (808 nm, 0.8 W/cm^2, 5 mins), and CUR/IR780@SMEDDS+NIR. (**E**) Quantitative analysis in 4T1 cells: (a) wound healing assay, (b) transwell migration assay, and (c) invasion assay. Photographs of the transwell migration assay (**F**) and invasion assay (**G**) with 4T1 cells treated with control, IR780, CUR@SMEDDS, CUR/IR780@SMEDDS, control+NIR, IR780+NIR, and CUR/IR780@SMEDDS+NIR. Data are represented as means±SD (n=5).

invasion of breast cancer cells by modulating multiple signaling pathways,[47–49] attributable to effects on expression of NF-κB p105, COX-2, and MMP9. In addition, anti-invasion effect of free IR780 to 4T1 cells was similar with the previous report,[50] suggesting the contribution of phototherapy on suppressing the tumor cell migration. Taken together, these findings indicate that CUR/IR780@SMEDDS markedly inhibited migration and invasion of 4T1 cells, implying that CUR/IR780@SMEDDS could potentially suppress breast cancer metastasis in vivo.

In vivo bioavailability

As enhanced bioavailability is a major condition for improving therapeutic efficacy, we compared CUR/IR780@SMEDDS bioavailability with that of suspensions prepared by dispersing curcumin and IR780 in 0.5% CMC-Na. Plasma concentration-time profiles for gavage administration of CUR/IR780@SMEDDS and suspensions in rats are shown in Figure 5A and B, whereas pharmacokinetic parameters are listed in Table 1. Significant differences in C_{max}, T_{max}, and AUC were observed between the groups. CUR/IR780@SMEDDS showed the highest C_{max} and AUC, with relative bioavailability of 743.7% and 307.0% for curcumin and IR780, respectively, indicating that CUR/IR780@SMEDDS significantly improved oral absorption of curcumin and IR780. Additionally, MRT of CUR/IR780@SMEDDS was significantly longer than that of suspensions, indicating a longer retention time of

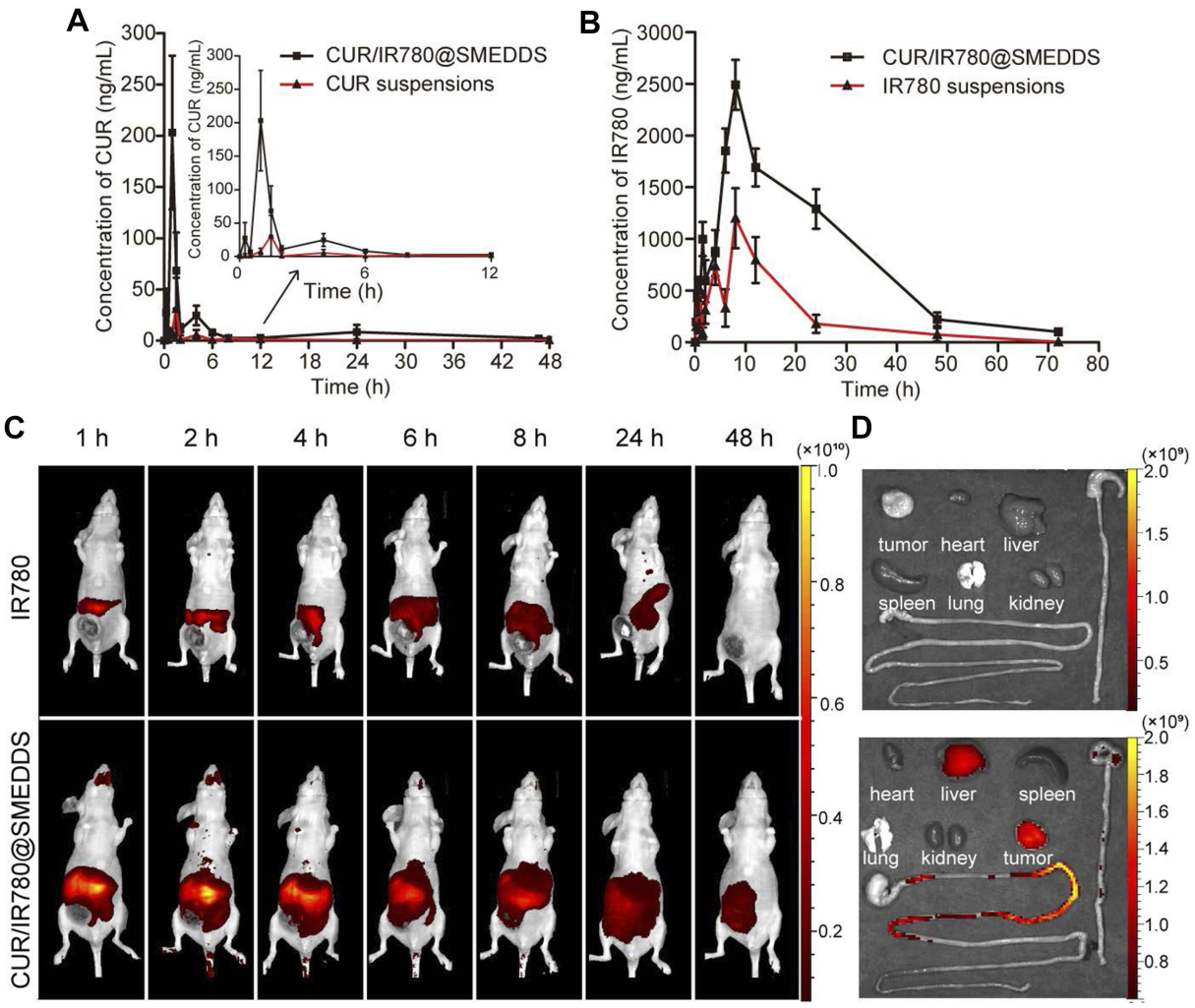

Figure 5 In vivo bioavailability and distribution study. (**A**) Plasma concentration-time curve of curcumin (CUR) in rats after oral administration of CUR suspensions and CUR/IR780@SMEDDS. (**B**) Plasma concentration-time curve of IR780 in rats after oral administration of IR780 suspensions and CUR/IR780@SMEDDS. Data are represented as means±SD (n=5). (**C**) Representative fluorescence images of rats treated with IR780 dispersions and CUR/IR780@SMEDDS at predetermined time points. (**D**) Representative fluorescence images of isolated tumors and organs, including the gastrointestinal tract.

Table 1 Pharmacokinetic parameters of curcumin (CUR) and IR780 after oral administration of CUR/IR780@SMEDDS, CUR suspensions, or IR780 suspensions in rats (n=5). Data are expressed as mean±SD.

Parameters	CUR		IR780	
	CUR suspensions	CUR/IR780 @SMEDDS	IR780 suspensions	CUR/IR780 @SMEDDS
AUC_{0-t} (μg·h/L)	58.96±37.81	438.46±367.80	18.85±13.49	57.88±13.65
$AUC_{0-\infty}$(μg·h/L)	78.77±29.16	462.23±374.35	18.86±13.48	59.31±13.85
MRT_{0-t} (h)	4.70±1.40	9.93±4.67	13.10±3.98	19.73±2.30
$MRT_{0-\infty}$ (h)	5.99±1.30	12.45±6.07	13.54±3.78	22.05±2.44
T_{max} (h)	3.10±2.22	0.95±0.45	9.33±2.07	7.67±0.82
CLz/F (L/h/kg)	1064.76±1493.15	257.01±163.05	0.78±0.48	0.18±0.04
C_{max} (μg/L)	44.76±61.03	247.44±129.74	1.32±0.58	2.61±0.46

SMEDDS in systemic circulation. IR780 was reported to be rapidly cleared from systemic circulation,[51] whereas SMEDDS formulations would allow accumulation of IR780 at the primary tumor and metastatic sites.

In vivo fluorescence imaging and biodistribution analysis

To analyze in vivo distribution and verify anti-metastatic potential of CUR/IR780@SMEDDS, in vivo fluorescence imaging was performed. IR780 fluorescence was recorded at predetermined time points after oral administration of CUR/IR780@SMEDDS. Whole animal fluorescence imaging showed that the control IR780 group produced almost no obvious fluorescence signals after 1 hr (Figure 5C). In contrast, strong fluorescence was observed in the group treated with CUR/IR780@SMEDDS, likely due to the rapid absorption of IR780 loaded in SMEDDS (Figure 5D). Fluorescence intensity decreased gradually and no obvious fluorescence was observed in IR780 suspension group after 48 hrs because of IR780 systemic clearance. In contrast, in animals treated with SMEDDS, fluorescence persisted longer, and was detectable even after 48 hrs. Passive IR780 tumor accumulation was further verified by fluorescence imaging of excised tissues (Figure 5D). IR780 tumor accumulation was significantly higher in animals treated with CUR/IR780@SMEDDS. CUR/IR780@SMEDDS group showed improved distribution of fluorescence in the gastrointestinal tract, especially at the jejunum, which is proposed as the main absorption site for IR780, indicating higher IR780 amounts available for systemic absorption in this group. This result supports the whole animal fluorescence imaging; CUR/IR780@SMEDDS treatment maintained stronger and longer-lasting IR780 fluorescence than that of control. Combined with the results of pharmacokinetic studies, these data indicate that CUR/IR780@SMEDDS achieved improved in vivo IR780 bioavailability.

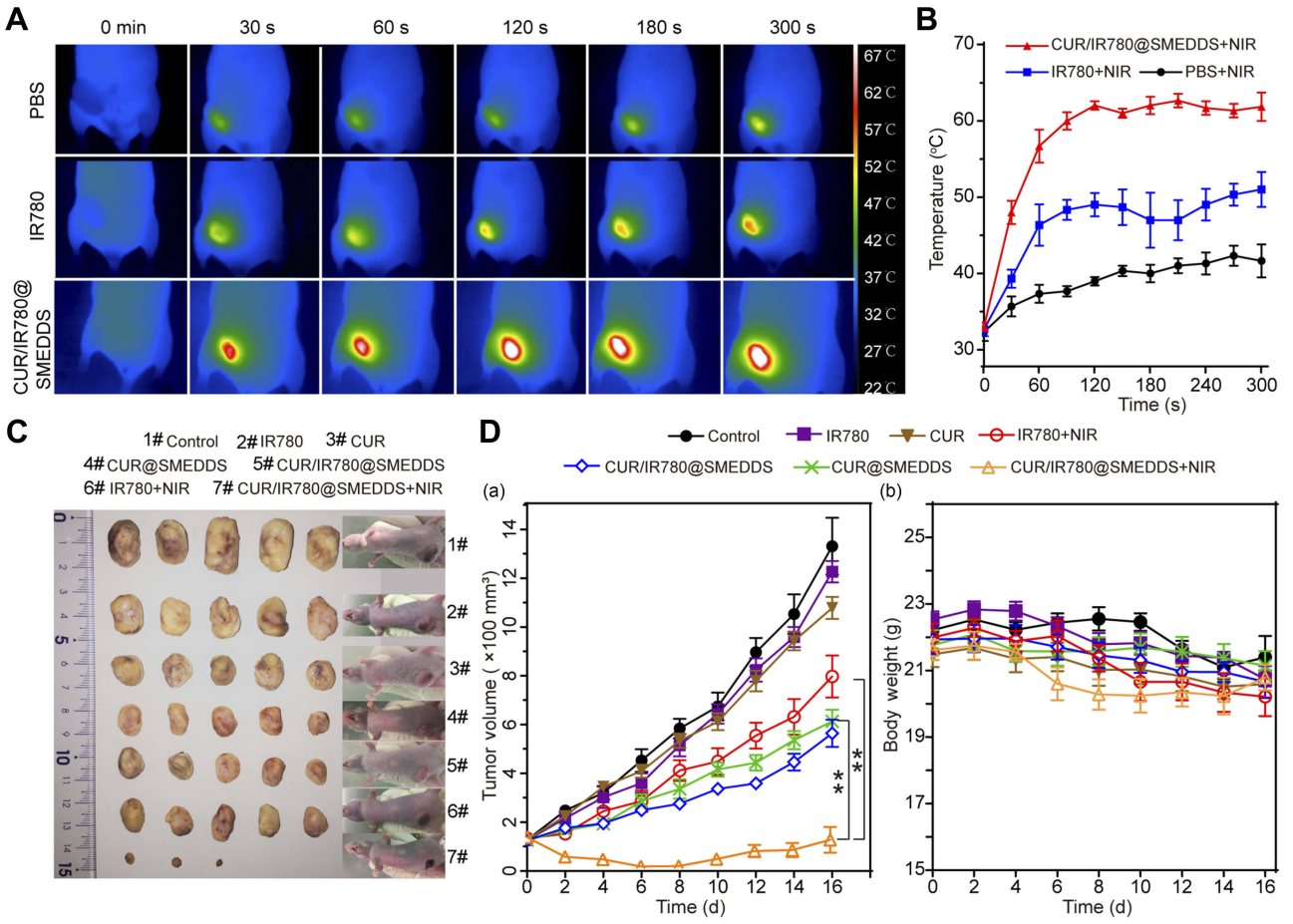

Figure 6 In vivo antitumor effects. (**A**) Photothermal images of 4T1 tumor-bearing nude mice treated with PBS, IR780, and CUR/IR780@SMEDDS under NIR laser irradiation. (**B**) Tumor temperature-time curve after NIR irradiation (n=3). (**C**) Photographs of tumors and 4T1 tumor-bearing nude mice treated with control, IR780, CUR, IR780+NIR, CUR/IR780@SMEDDS, CUR@SMEDDS, and CUR/IR780@SMEDDS+NIR 16 days after administration. (**D**) (a) Tumor volume in nude mice treated with control, IR780, CUR, CUR@SMEDDS, CUR/IR780@SMEDDS, IR780+NIR, and CUR/IR780@SMEDDS+NIR; $^{**}p<0.01$. (b) Body weight change of tumor-bearing mice. Data are represented as mean±SD (n=7).

Photothermal efficacy of CUR/IR780@SMEDDS in vivo

Photothermal efficacy was evaluated in 4T1 tumor-bearing mice to further demonstrate the potential of CUR/IR780@SMEDDS in the treatment of metastatic breast cancer. IR images were taken after 5-min laser irradiation and corresponding temperatures were recorded. As shown in Figure 6A and B, in IR780 and CUR/IR780@SMEDDS groups temperature rapidly increased for the first 120 s, before leveling off. Tumor temperature reached 50°C and 60°C in the two groups, respectively, with 60°C sufficient for tumor ablation. Only slight changes in temperature were observed in the control group. These results suggest that CUR/IR780@SMEDDS possesses potent in vivo photothermal efficacy.

In vivo therapeutic efficacy

In vivo therapeutic efficacy of CUR/IR780@SMEDDS against metastatic breast cancer was assessed on 4T1 tumor-bearing mice. As shown in Figure 6C, tumor volumes of animals treated with free IR780, free curcumin, and IR780 combined with NIR irradiation showed no significant differences compared with the control group, in which tumor volumes increased rapidly, reaching 6–10 times starting volumes by day 16 (Figure 6D(a)). These results indicated that these three treatments failed to achieve desirable antitumor effects, possibly because of poor oral absorption and low bioavailability of the compounds. In the same experiment, CUR/IR780@SMEDDS showed enhanced tumor inhibition compared with CUR@SMEDDS, indicating that IR780 contributes to antitumor effects when introduced into SMEDDS. The most remarkable tumor inhibition effects were observed in mice receiving CUR/IR780@SMEDDS combined with NIR irradiation, in which gradual decrease in tumor size was observed until day 8. After day 8, tumor recurrence was observed in three mice in this group, however, tumor volumes remained lower than initial volumes. Taken together, these data suggest that CUR/IR780@SMEDDS treatment combined with NIR irradiation showed remarkable antitumor efficacy compared with chemotherapy or phototherapy alone. No notable body weight loss was observed in any group during the 16 days of treatment (Figure 6D(a)), indicating a lack of significant physiological toxicity of the treatments at the dose used (Figure 6D(b)).

Although oral IR780 loaded nanostructured lipid carrier designed for photothermal therapy has been reported previously, how to further improve the therapeutic efficiency and assure safety remains worthy of investigation. Firstly, given the limited penetration depth of NIR dye, sole

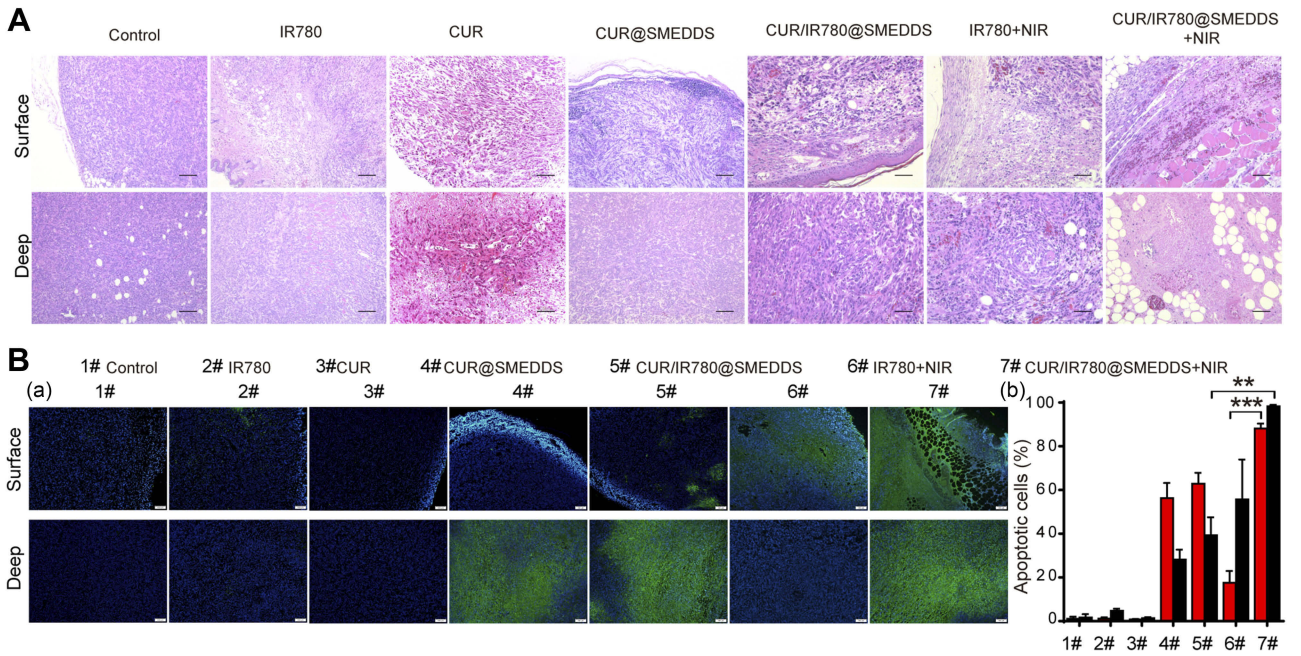

Figure 7 (**A**) Histological examination (scale 200 μm) and (**B**) TUNEL analysis of tumor tissues treated with control, IR780, CUR, CUR@SMEDDS, CUR/IR780@SMEDDS, IR780+NIR, and CUR/IR780@SMEDDS+NIR 16 days after administration. "Surface" and "Deep" labeled rows represent H&E images of superficial and deep tumor tissue regions, respectively. (a) TUNEL assay images and (b) quantitative analysis of fluorescence intensity in apoptotic cells (mean±SD, n=5).

phototherapy may be ineffective to the inner section of the tumor especially when the tumor becomes larger. Therefore, it is rational to understand the better therapeutic efficiency in CUR/IR780@SMEDDS than the pure IR780 by NIR treatment. Combination of photothermal therapy with chemotherapy is more valuable in the treatment of metastatic breast cancer. Secondly, one of the limitations for IR780 application is its acute toxicity (1 mg/kg to mice by intravenous administration[52]). To assure the safety of IR780, dose reduction is desirable. Compared to previously reported IR780 nanostructured lipid carrier designed for photothermal therapy, CUR/IR780@SMEDDS demonstrated superior effects at a reduced dose (IR780 5 mg/kg vs 6 mg/kg) and lower NIR power density (0.8 W/cm^2 vs 2 W/cm^2) due to improved IR780 absorption and facilitated chemotherapeutic effect.

To further demonstrate cellular antitumor activity of CUR/IR780@SMEDDS, histological examination and apoptosis assays were performed. As deeper segments of tumor tissues could be shielded from photothermal treatment because of limited light penetration,[5] both superficial and deep tumor tissue regions were H&E stained (Figure 7A). Control group tumors showed numerous tumor cells with preserved tissue structure. Free IR780 treatment combined with NIR irradiation was not cytotoxic to tumor cells in deeper tissue regions, consistent with a previous report.[30] After CUR/IR780@SMEDDS treatment in the absence of NIR irradiation, notable tumor tissue structure and invasion of tumor cells to soft tissues were observed in superficial tissue sections, whereas considerable necrosis and infiltration of inflammatory cells occurred in deep tissue regions. In contrast,

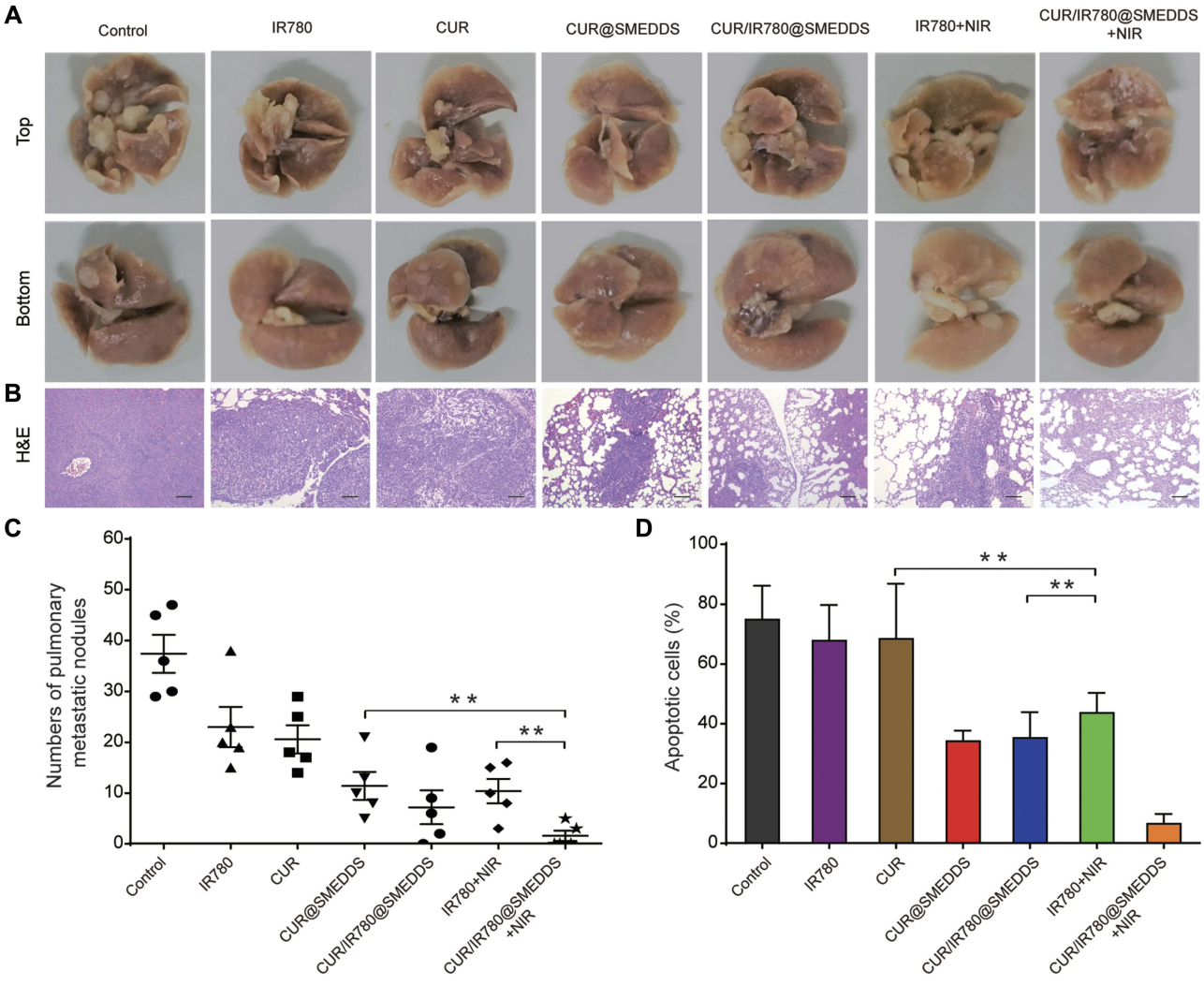

Figure 8 (**A**) Photographs and (**B**) histological examination of pulmonary metastatic nodules in nude mice treated with control, IR780, CUR, CUR@SMEDDS, CUR/IR780@SMEDDS, IR780+NIR, and CUR/IR780@SMEDDS+NIR. (**C**) Number of pulmonary metastatic nodules in nude mice after treatments. (**D**) Pulmonary metastatic area of nude mice after treatments. Data are represented as mean±SD of five animals. ** p<0.01.

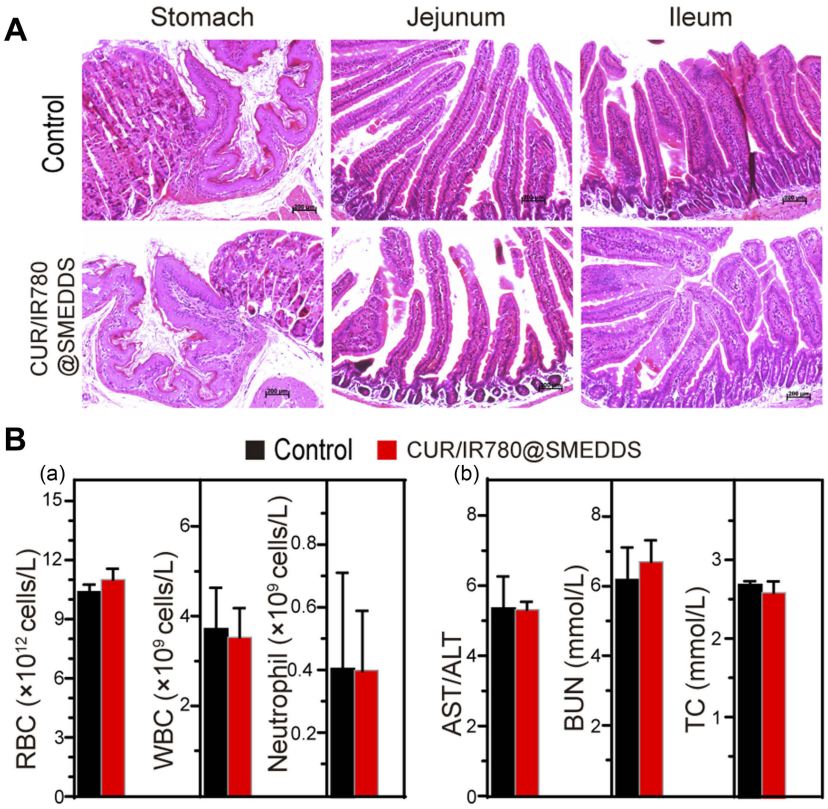

Figure 9 (**A**) Histological examination of stomach, jejunum, and ileum. (**B**) (a) Hematological and (b) biochemical parameters of liver and kidney function in mice treated with control and CUR/IR780@SMEDDS (means±SD, n=5).

CUR/IR780@SMEDDS treatment combined with NIR irradiation resulted in no observable tumor tissue sections, with local inflammatory cell infiltration occurring in both superficial and deep tissue regions. As shown in Figure 7B, apoptosis was very rarely observed in control groups, whereas in IR780 and curcumin group slight apoptosis was observable in superficial and deep tissue sections, respectively. In CUR@SMEDDS, CUR/IR780@SMEDDS, and CUR/IR780@SMEDDS+NIRand IR780+NIR group, apoptosis was significantly more pronounced (Figure 7B). The CUR/IR780@SMEDDS group presented cavities in superficial tissue structures, possibly caused by high temperatures resulting from the photothermal effect, with considerable degree of apoptosis occurring in deep tissues. These results illustrate improved antitumor effects of combined photo- and chemotherapy.

To evaluate the efficacy of CUR/IR780@SMEDDS in inhibiting lung metastasis, we determined the number of pulmonary metastatic nodules and histopathologically analyzed lung sections from 4T1 tumor-bearing mice (Figure 8A). IR780 and curcumin treatment induced approximately onefold decrease in the number of metastatic nodules, compared to control (Figure 8C). Enhanced inhibition was observed in all SMEDDS groups ($p<0.05$), possibly because SMEDDS improved in vivo absorption of curcumin and IR780. Additionally, metastatic nodules were rarely observed in the lungs of CUR/IR780@SMEDDS+NIR group mice; the strongest anti-metastatic effects were observed in this group. H&E staining (Figure 8B) indicated that smaller areas of metastasis foci were observed in the SMEDDS groups compared to free curcumin and IR780 groups, with CUR/IR780@SMEDDS group showing the smallest foci area (Figure 8D), consistent with the nodule counting results. These findings indicate that CUR/IR780@SMEDDS combined with NIR irradiation achieved the highest inhibition of 4T1 tumor metastasis among the treatments studied.

Preliminary safety evaluation in mice

In addition to monitoring mice body weight, we evaluated histopathological, biochemical, and hematologic parameters. H&E staining indicated no significant signs of organ damage to heart, liver, spleen, and kidney in treated mice, compared to organs of control animals (Figure S6). Gastrointestinal tract

histopathological findings of CUR/IR780@SMEDDS and control group are shown in Figure 9A. No obvious squamous epithelial cell proliferation, prominent keratinization, or obvious lesions were observed in the stomach. In jejunum and ileum, the shape of intestinal villi was unaltered and no congestion, proliferation, heteromorphosis, or inflammatory infiltration was observed. These results indicate that CUR/IR780@SMEDDS lacks gastrointestinal toxicity. Aspartate aminotransferase, alanine aminotransferase, blood urea nitrogen, and total cholesterol levels (Figure 9B) suggested no liver or kidney dysfunctions. Additionally, no significant changes in white blood cell, red blood cell, and neutrophil levels were observed in CUR/IR780@SMEDDS-treated animals compared to levels in the control group. These results suggest negligible side effects of CUR/IR780@SMEDDS in vivo, possibly because of preferential accumulation of IR780 and curcumin in tumors and low treatment dose used in this study.

Conclusion

In summary, CUR/IR780@SMEDDS improved cellular uptake in Caco-2 cells and enhanced oral bioavailability of curcumin and IR780 in rats. Additionally, CUR/IR780@SMEDDS showed enhanced cytotoxicity and inhibited migration and invasion of 4T1 cells when combined with NIR irradiation. Improved therapeutic effect of the designed SMEDDS was also demonstrated in vivo, in 4T1 tumor-bearing nude mice, suggesting potential benefits of this formulation in treating metastatic breast cancer. These results suggest CUR/IR780@SMEDDS as a safe and promising addition to combined cancer therapy approaches, suitable for oral administration.

Acknowledgment

This work was supported by the National Natural Science Foundation of China [Grant No. 81773913 and 81303232].

Disclosure

The authors report no conflicts of interest in this work.

References

1. Gennari A, Conte P, Rosso R, Orlandini C, Bruzzi P. Survival of metastatic breast carcinoma patients over a 20-year period. *Cancer*. 2005;104:1742–1750. doi:10.1002/cncr.21359
2. Valastyan S, Weinberg RA. Tumor metastasis: molecular insights and evolving paradigms. *Cell*. 2011;147:275–292. doi:10.1016/j.cell.2011.09.024
3. Safwat S, Hathout RM, Ishak RA, Mortada ND. Augmented simvastatin cytotoxicity using optimized lipid nanocapsules: a potential for breast cancer treatment. *J Liposome Res*. 2017;27(1):1–10. doi:10.3109/08982104.2015.1137313
4. Trovo M, Furlan C, Polesel J, et al. Radical radiation therapy for oligometastatic breast cancer: results of a prospective phase II trial. *Radiother Oncol*. 2017;126(1):177–180. doi:10.1016/j.radonc.2017.08.032
5. Zhou J, Lu Z, Zhu X, et al. NIR photothermal therapy using polyaniline nanoparticles. *Biomaterials*. 2013;34(37):9584–9592. doi:10.1016/j.biomaterials.2013.08.075
6. García Calavia P, Chambrier I, Cook MJ, Haines AH, Field RA, Russell DA. Targeted photodynamic therapy of breast cancer cells using lactose-phthalocyanine functionalized gold nanoparticles. *J Colloid Interface Sci*. 2017;512:249–259. doi:10.1016/j.jcis.2017.10.030
7. Abozeid SM, Hathout RM, Abou-Aisha K. Silencing of the metastasis-linked gene, AEG-1, using siRNA-loaded cholamine surface-modified gelatin nanoparticles in the breast carcinoma cell line MCF-7. *Colloids Surf B*. 2016;145:607–616. doi:10.1016/j.colsurfb.2016.05.066
8. Hathout RM, Metwally AA, El-Ahmady SH, et al. Dual stimuli-responsive polypyrrole nanoparticles for anticancer therapy. *J Drug Deliv Sci Technol*. 2018;47:176–180. doi:10.1016/j.jddst.2018.07.002
9. Li WT, Peng JR, Tan LW, et al. Mild photothermal therapy/photodynamic therapy/chemotherapy of breast cancer by Lyp-1 modified Docetaxel/IR820 Co-loaded micelles. *Biomaterials*. 2016;106:119–133. doi:10.1016/j.biomaterials.2016.08.016
10. Cherukula K, Lekshmi KM, Uthaman S, Cho K, Cho CS, Park IK. Multifunctional inorganic nanoparticles: recent progress in thermal therapy and imaging. *Nanomaterials*. 2016;6(4):76. doi:10.3390/nano6040076
11. Gong H, Dong Z, Liu Y, et al. Engineering of multifunctional nanomicelles for combined photothermal and photodynamic therapy under the guidance of multimodal imaging. *Adv Funct Mater*. 2015;24:6492–6502. doi:10.1002/adfm.201401451
12. Zhang E, Luo S, Tan X, Shi C. Mechanistic study of IR-780 dye as a potential tumor targeting and drug delivery agent. *Biomaterials*. 2014;35:771–778. doi:10.1016/j.biomaterials.2013.10.033
13. Wang Y, Liu T, Zhang E, Luo S, Tan X, Shi C. Preferential accumulation of the near infrared heptamethine dye IR-780 in the mitochondria of drug-resistant lung cancer cells. *Biomaterials*. 2014;35:4116–4124. doi:10.1016/j.biomaterials.2014.01.061
14. Alves CG, Lima-Sousa R, de Melo-Diogo D, Louro RO, Correia IJ. IR780 based nanomaterials for cancer imaging and photothermal, photodynamic and combinatorial therapies. *Int J Pharm*. 2018;542:164–175. doi:10.1016/j.ijpharm.2018.03.020
15. Chen G, Wang K, Zhou Y, et al. Oral Nanostructured lipid carriers loaded with near-infrared dye for image-guided photothermal therapy. *ACS Appl Mater Interfaces*. 2016;8(38):25087–25095. doi:10.1021/acsami.6b07425
16. Li H, Wang K, Yang X, et al. Dual-function nanostructured lipid carriers to deliver IR780 for breast cancer treatment: anti-metastatic and photothermal anti-tumor therapy. *Acta Biomater*. 2017;53:399–413. doi:10.1016/j.actbio.2017.01.070
17. Zheng M, Yu CE, Ma Y, et al. Single-step assembly of DOX/ICG loaded lipid–polymer nanoparticles for highly effective chemo-photothermal combination therapy. *ACS Nano*. 2013;7(3):2056–2067. doi:10.1021/nn400334y
18. Liao J, Li W, Peng J, et al. Combined cancer photothermal-chemotherapy based on doxorubicin/gold nanorod-loaded polymersomes. *Theranostics*. 2015;5(4):345–356. doi:10.7150/thno.10731
19. Zhou H, Beevers CS, Huang S. Targets of curcumin. *Curr Drug Targets*. 2011;12(3):332–347.

20. Kunnumakkara AB, Anand P, Aggarwal BB. Curcumin inhibits proliferation, invasion, angiogenesis and metastasis of different cancers through interaction with multiple cell signaling proteins. *Cancer Lett*. 2008;269(2):199–225. doi:10.1016/j.canlet.2008.03.009
21. Gallardo M, Calaf GM. Curcumin inhibits invasive capabilities through epithelial mesenchymal transition in breast cancer cell lines. *Int J Oncol*. 2016;49(3):1019–1027. doi:10.3892/ijo.2016.3598
22. Sharma RA, Mclelland HR, Hill KA, et al. Pharmacodynamic and pharmacokinetic study of oral Curcuma extract in patients with colorectal cancer. *Clin Cancer Res*. 2001;7(7):1894–1900.
23. Abdel-Hafez SM, Hathout RM, Sammour OA. Curcumin-loaded ultradeformable nanovesicles as a potential delivery system for breast cancer therapy. *Colloids Surf B*. 2018;167:63–72. doi:10.1016/j.colsurfb.2018.03.051
24. Metwally AA, El-Ahmady SH, Hathout RM. Selecting optimum protein nano-carriers for natural polyphenols using chemoinformatics tools. *Phytomedicine*. 2016;23(14):1764–1770. doi:10.1016/j.phymed.2016.10.020
25. Abdel-Hafez SM, Hathout RM, Sammour OA. Tracking the transdermal penetration pathways of optimized curcumin-loaded chitosan nanoparticles via confocal laser scanning microscopy. *Int J Biol Macromol*. 2018;108:753–764. doi:10.1016/j.ijbiomac.2017.10.170
26. Luo C, Sun J, Du Y, He Z. Emerging integrated nanohybrid drug delivery systems to facilitate the intravenous-to-oral switch in cancer chemotherapy. *J Control Release*. 2014;176:94–103. doi:10.1016/j.jconrel.2013.12.030
27. Cardoso F, Colleoni M, Leo AD, et al. Oral chemotherapy in advanced breast cancer: expert perspectives on its role in clinical practice. *Cancer Treat Commun*. 2016;6:S1–S10. doi:10.1016/S2213-0896(16)06001-1
28. Date AA, Hanes J, Ensign LM. Nanoparticles for oral delivery: design, evaluation and state-of-the-art. *J Control Release*. 2016;240:504–526. doi:10.1016/j.jconrel.2016.06.016
29. Qin J, Wang W, Sarkar S, Zhang R. Oral delivery of anti-MDM2 inhibitor SP141-loaded FcRn-targeted nanoparticles to treat breast cancer and metastasis. *J Control Release*. 2016;237:101–114. doi:10.1016/j.jconrel.2016.07.008
30. Wei W, Lv PP, Chen XM, et al. Codelivery of mTERT siRNA and paclitaxel by chitosan-based nanoparticles promoted synergistic tumor suppression. *Biomaterials*. 2013;34(15):3912–3923. doi:10.1016/j.biomaterials.2013.02.030
31. Kohli K, Chopra S, Dhar D, Arora S, Khar RK. Self-emulsifying drug delivery systems: an approach to enhance oral bioavailability. *Drug Discov Today*. 2010;15(21–22):958–965. doi:10.1016/j.drudis.2010.08.007
32. Shukla M, Jaiswal S, Sharma A, et al. A combination of complexation and self-nanoemulsifying drug delivery system for enhancing oral bioavailability and anticancer efficacy of curcumin. *Drug Dev Ind Pharm*. 2016;43(5):847–861. doi:10.1080/03639045.2016.1239732
33. Fagir W, Hathout RM, Sammour OA, et al. Self-microemulsifying systems of finasteride with enhanced oral bioavailability: multivariate statistical evaluation, characterization, spray-drying and in vivo studies in human volunteers. *Nanomedicine*. 2015;10(22):3373–3389.
34. Yehia R, Hathout RM, Attia DA, Elmazar MM, Mortada ND. Anti-tumor efficacy of an integrated methyl dihydrojasmonate transdermal microemulsion system targeting breast cancer cells: in vitro and in vivo studies. *Colloids Surf B*. 2017;155:512–521. doi:10.1016/j.colsurfb.2017.04.031
35. Sinha S, Khan S, Shukla S, et al. Cucurbitacin B inhibits breast cancer metastasis and angiogenesis through VEGF-mediated suppression of FAK/MMP-9 signaling axis. *Int J Biochem Cell Biol*. 2016;77(Pt A):41–56. doi:10.1016/j.biocel.2016.05.014
36. Li J, Oupický D. Effect of biodegradability on CXCR4 antagonism, transfection efficacy and antimetastatic activity of polymeric Plerixafor. *Biomaterials*. 2014;35(21):5572–5579. doi:10.1016/j.biomaterials.2014.03.047
37. Yue C, Liu P, Zheng M, et al. IR-780 dye loaded tumor targeting theranostic nanoparticles for NIR imaging and photothermal therapy. *Biomaterials*. 2013;34(28):6853–6861. doi:10.1016/j.biomaterials.2013.05.071
38. Pais-Silva C, de Melo-Diogo D, Correia IJ. IR780-loaded TPGS-TOS micelles for breast cancer photodynamic therapy. *Eur J Pharm Biopharm*. 2017;113:108–117. doi:10.1016/j.ejpb.2017.01.002
39. Khan J, Alexander A, Ajazuddin SS, Saraf S. Recent advances and future prospects of phyto-phospholipid complexation technique for improving pharmacokinetic profile of plant actives. *J Control Release*. 2013;168(1):50–60. doi:10.1016/j.jconrel.2013.02.025
40. Maiti K, Mukherjee K, Gantait A, Saha BP, Mukherjee PK. Curcumin-phospholipid complex: preparation, therapeutic evaluation and pharmacokinetic study in rats. *Int J Pharm*. 2007;330(1–2):155–-163. doi:10.1016/j.ijpharm.2006.09.025
41. Jelezova I, Drakalska E, Momekova D, et al. Curcumin loaded pH-sensitive hybrid lipid/block copolymer nanosized drug delivery systems. *Eur J Pharm Sci*. 2015;78:67–78. doi:10.1016/j.ejps.2015.07.005
42. Zhang C, Wang S, Xiao J, et al. Sentinel lymph node mapping by a near-infrared fluorescent heptamethine dye. *Biomaterials*. 2010;31(7):1911–1917. doi:10.1016/j.biomaterials.2009.11.061
43. Shibu ES, Hamada M, Murase N, Biju V. Nanomaterials formulations for photothermal and photodynamic therapy of cancer. *J Photoch Photobio C*. 2013;15:53–72. doi:10.1016/j.jphotochemrev.2012.09.004
44. Lian HB, Wu JH, Hu YQ, Guo HQ. Self-assembled albumin nanoparticles for combination therapy in prostate cancer. *Int J Nanomedicine*. 2017;12:7777–7787. doi:10.2147/IJN.S144634
45. Palaosuay R, Martínsaavedra FM, Rosa AM, et al. Photothermal and photodynamic activity of polymeric nanoparticles based on α-tocopheryl succinate-RAFT block copolymers conjugated to IR-780. *Acta Biomater*. 2017;57:70–84. doi:10.1016/j.actbio.2017.05.028
46. Yan F, Duan W, Li Y, et al. NIR-laser-controlled drug release from DOX/IR-780-loaded temperature-sensitive-liposomes for chemo-photothermal synergistic tumor therapy. *Theranostics*. 2016;6(13):2337–2351. doi:10.7150/thno.14937
47. Narasimhan M, Ammanamanchi S. Curcumin blocks RON tyrosine kinase-mediated invasion of breast carcinoma cells. *Cancer Res*. 2008;68(13):5185–5192. doi:10.1158/0008-5472.CAN-07-6883
48. Huang T, Chen Z, Fang L. Curcumin inhibits LPS-induced EMT through downregulation of NF-κB-Snail signaling in breast cancer cells. *Oncol Rep*. 2013;29(1):117–124. doi:10.3892/or.2012.2080
49. Zong H, Wang F, Fan QX, Wang LX. Curcumin inhibits metastatic progression of breast cancer cell through suppression of urokinase-type plasminogen activator by NF-kappa B signaling pathways. *Mol Biol Rep*. 2012;39(4):4803–4808. doi:10.1007/s11033-011-1273-5
50. Cao HQ, Zou LL, He B, et al. Albumin biomimetic nanocorona improves tumor targeting and penetration for synergistic therapy of metastatic breast cancer. *Adv Funct Mater*. 2017;27(11):1605679. doi:10.1002/adfm.201605679
51. Han H, Wang J, Chen T, Yi L, Jin Q, Ji J. Enzyme-sensitive gemcitabine conjugated albumin nanoparticles as a versatile theranostic nanoplatform for pancreatic cancer treatment. *J Colloid Interface Sci*. 2017;507:217–224. doi:10.1016/j.jcis.2017.07.047
52. Jiang C, Cheng H, Yuan A, Tang X, Wu J, Hu Y. Hydrophobic IR780 encapsulated in biodegradable human serum albumin nanoparticles for photothermal and photodynamic therapy. *Acta Biomater*. 2015;14:61–69. doi:10.1016/j.actbio.2014.11.041

Supplemental materials

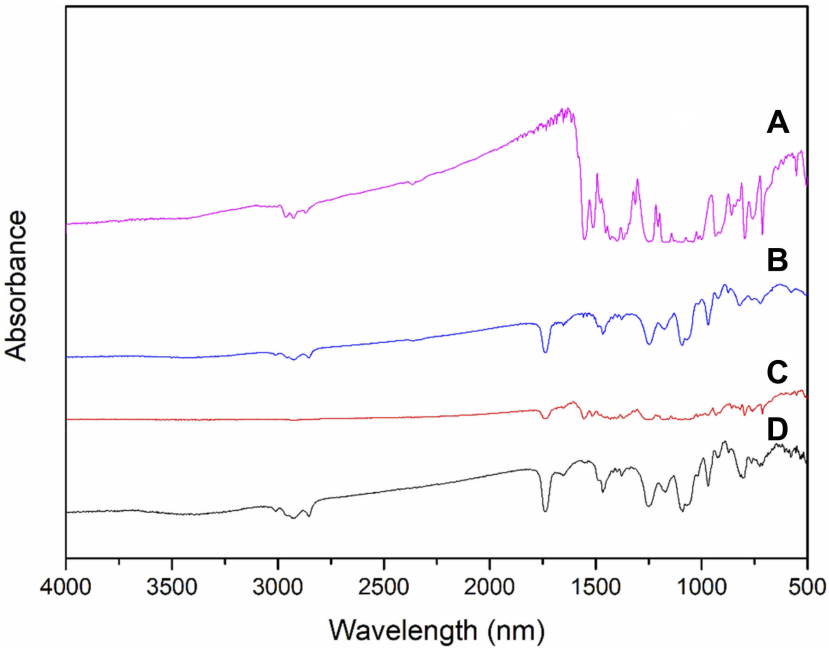

Figure S1 FTIR spectra of (**A**) Raw IR780, (**B**) PC, (**C**) physical mixture of IR780 and PC, and (**D**) IR780 PC formed by the phospholipid complex preparing process.

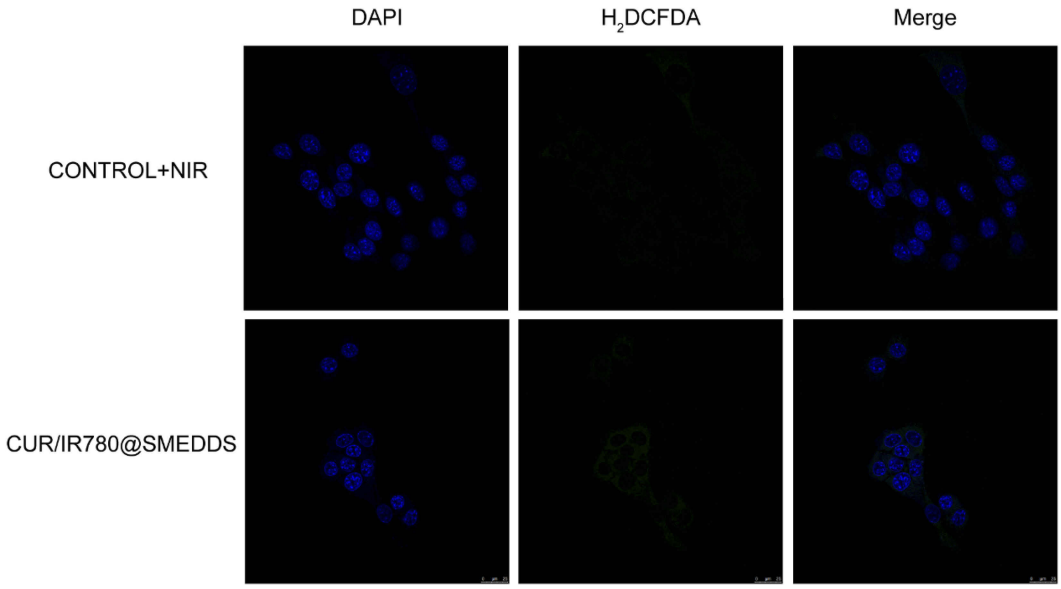

Figure S2 Confocal images of ROS generation by control under NIR irradiation (808 nm, 0.8 W/cm^2, 5 mins) and CUR@SMEDDS in 4T1 cells.

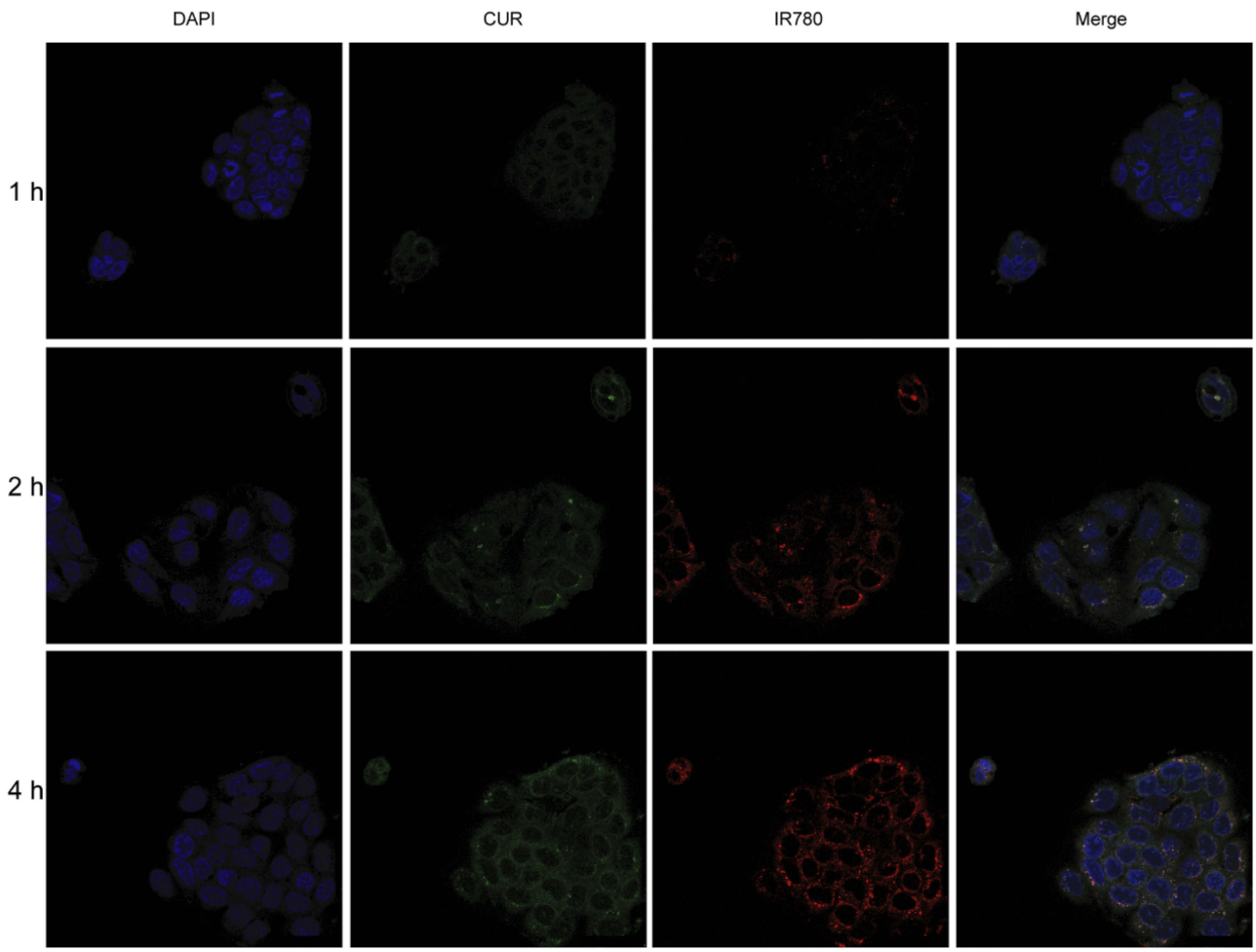

Figure S3 Confocal images of cellular uptake for CUR/IR780@SMEDDS in Caco-2 cells.

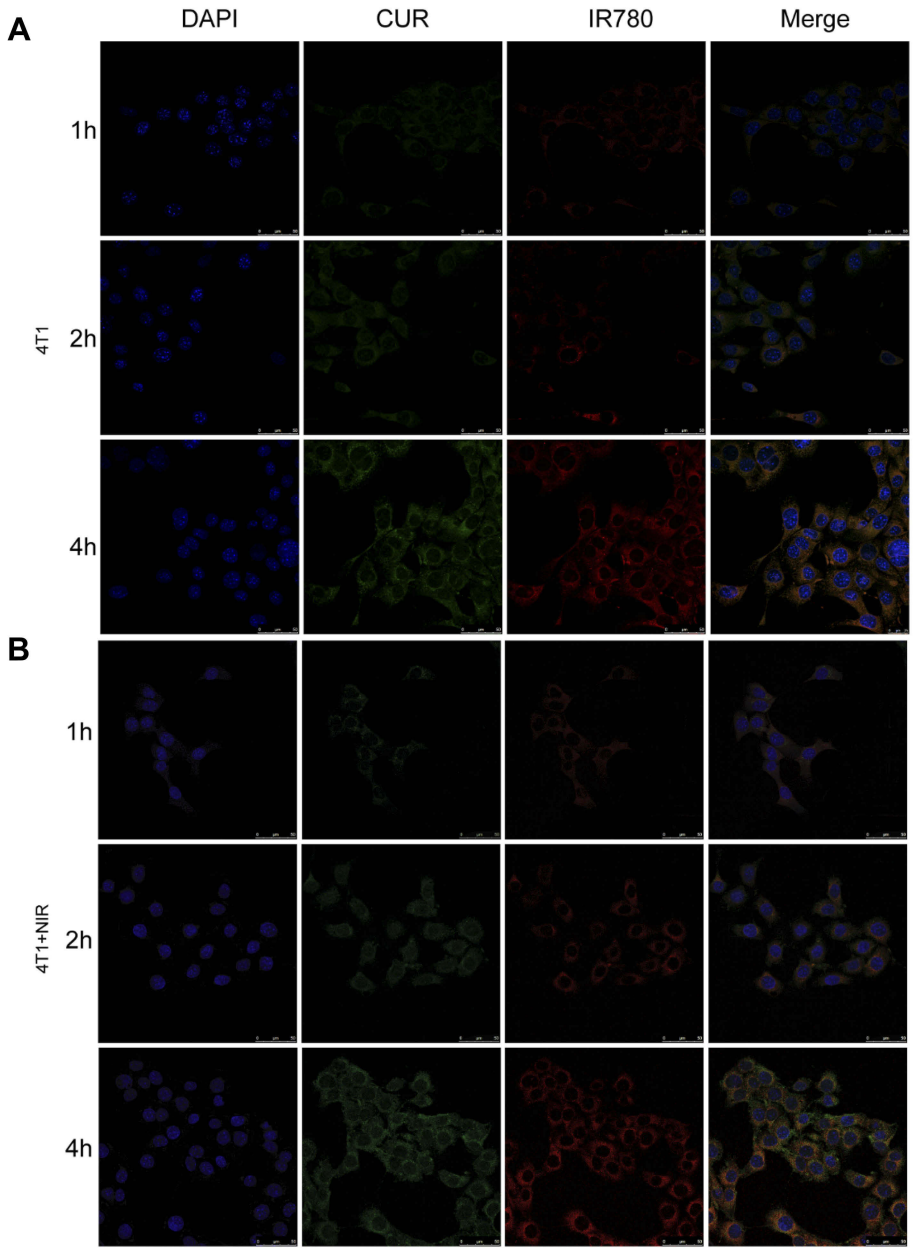

Figure S4 Confocal images of cellular uptake for CUR/IR780@SMEDDS in (**A**) 4T1 cells and (**B**) 4T1 cells under NIR irridiation (808 nm, 0.8 W/cm^2, 5 mins).

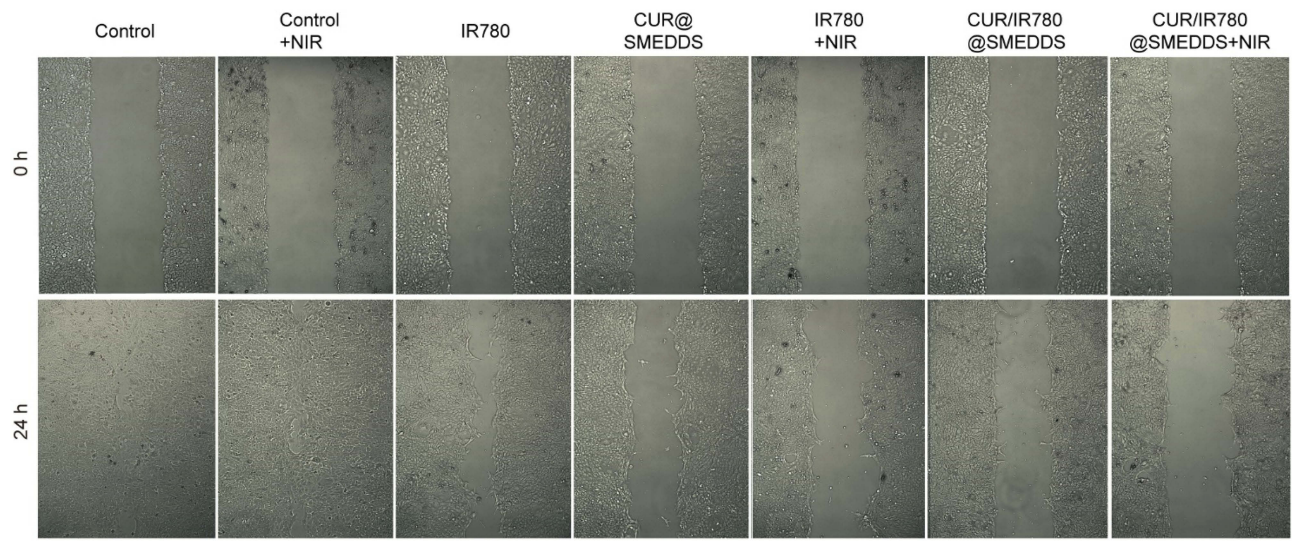

Figure S5 Photographs of the wound healing assay with 4T1 cells treated with control, IR780, CUR@SMEDDS, CUR/IR780@SMEDDS, control+NIR, IR780+NIR, and CUR/IR780@SMEDDS+NIR.

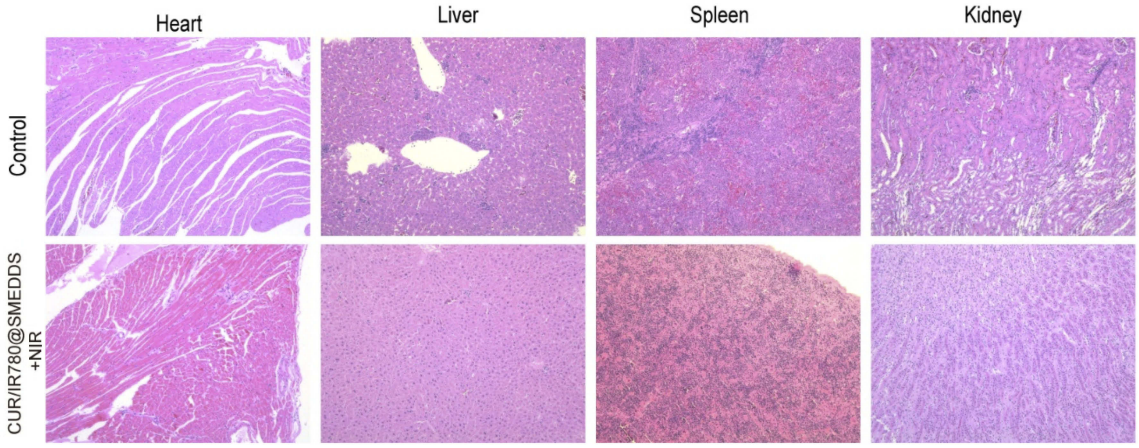

Figure S6 Histological examination of heart, liver, spleen, and kidney in tumor-bearing nude mice treated with control and CUR/IR780@SMEDDS+NIR.